Optimal Planning and Operation of Multi-type Flexible Resources Based on Differentiated Feature Matching in Regional Power Grid with High Proportion of Clean Energy

Jie Li, Xiaoming Liu, Zixuan Zheng, *Member*, *IEEE*, Xianyong Xiao, Shu Zhang, Hongzhi Gao, and Yongjun Zhou

***Abstract*—The optimal planning and operation of multi-type flexible resources (FRs) are critical prerequisites for maintaining power and energy balance in regional power grids with a high proportion of clean energy. However, insufficient consideration of the multi-dimensional and heterogeneous features of FRs, such as the regulation characteristics of diversified battery energy storage systems (BESSs), poses a challenge in economically relieving imbalance power and adequately sharing feature information between power supply and demand. In view of this disadvantage, an optimal planning and operation method based on differentiated feature matching through response capability characterization and difference quantification of FRs is proposed in this paper. In the planning stage, a model for the optimal planning of diversified energy storages (ESs) including Lithium-ion battery (Li-B), supercapacitor energy storage (SC-ES), compressed air energy storage (CAES), and pumped hydroelectric storage (PHS) is established. Subsequently, in the operating stage, the potential, direction, and cost of FR response behaviors are refined to match with the power and energy balance demand (PEBD) of power grid operation. An optimal operating algorithm is then employed to quantify the feature differences and output response sequences of multi-type FRs. The performance and effectiveness of the proposed method are demonstrated through comparative studies conducted on an actual regional power grid in northwest China. Analysis and simulation results illustrate that the proposed method can effectively highlight the advantages of BESSs compared with other ESs, and economically reduce imbalance power of the regional power grid under practical operating conditions.**

***Index Terms*—Regional power grid, planning and operation, energy storage, flexible resource, response capability, feature matching.**

Manuscript received: September 30, 2023; revised: December 12, 2023; accepted: February 8, 2024. Date of CrossCheck: February 8, 2024. Date of online publication: March 5, 2024.

This work was supported by the Science and Technology Major Project of Tibetan Autonomous Region of China (No. XZ202201ZD0003G).

J. Li, Z. Zheng (corresponding author), X. Xiao, S. Zhang, and Y. Zhou are with the College of Electrical Engineering, Sichuan University, Chengdu, China, and Y. Zhou is also with the State Grid Tibet Power Co., Ltd., Lhasa, China (e-mail: sculijie@163. com; scuzzx@163. com; xiaoxianyong@163. com; ZS20061621@163. com; xizang_zhouYJ@163.com).

X. Liu and H. Gao are with the State Grid Tibet Power Co., Ltd., Lhasa, China (e-mail: 83517573@qq.com; Gaohongzhi_XZ@163.com).

DOI: 10.35833/MPCE.2023.000741

I. Introduction

THE surging demand for flexible resources (FRs) in power grids with a high proportion of clean energy stems from their inherent intermittency and variability, crucial for maintaining power and energy balance [1], [2]. However, the conventional optimization approach for multi-type FRs primarily focuses on increasing the reserve capacity of thermal power and hydropower units, which is challenging to adapt to scenarios in power grids with a high proportion of clean energy [3], [4]. Therefore, there is an urgent need to fully explore the coordinated regulation capabilities of multi-type FRs [5]. Furthermore, by selecting the appropriate energy storage (ES) type to match power and energy balance demand (PEBD), the location and sizing of diversified ESs with varied regulation capabilities can enhance the operating stability and economic benefits of the power grid, facilitating the superior performance of ES technologies such as the Lithium-ion battery (Li-B) [6], [7]. However, solely relying on qualitative analysis of FR operations or considering a single type of ES often leads to conservative optimization results and generation curtailment [8], [9]. Besides, multi-type FRs comprising allocated battery energy storage systems (BESSs) exhibit significant differences in fundamental features including potential, direction, and cost of FR response behaviors. Neglecting these differences and simply combining multi-type FRs without sequence can hinder optimal operating performance and economic benefits in regional power grids [10], [11].

Numerous studies have concentrated on optimizing the planning of diversified ESs and coordinating the operation of multi-type FRs in power grids, especially BESSs. As a pivotal FR component to satisfy the PEBD of the power grid, the strategic placement and sizing of ESs are important to achieve superior operating performance and economic benefits [12]. Reference [13] proposes a formulation to determine the sizing and siting of BESSs in a power system with high penetration of renewables, aiming to reduce operating costs, enhance clean energy utilization, and mitigate power curtailment. In [14], a two-step optimal planning model is proposed for stationary ES systems and mobile ES systems, considering the mobility and supporting capabilities of the latter. Additionally, [15] achieves optimal planning of hybrid ES capacity, incorporating BESSs, through equilibrium control and dynamic optimization algorithms, considering various wind and solar irradiance combinations, sampling intervals, and power station numbers. In [16], a hybrid power management approach is developed for electric vehicle batteries and local conventional BESSs, utilizing model predictive control for power grid frequency regulation. While the aforementioned optimal allocation strategies of ESs analyze their crucial role in suppressing power and frequency fluctuations in regional power grids, they predominantly focus on BESSs, thereby neglecting the diverse regulation capabilities of other ES types, posing a challenge in achieving economic power balance. Reference [17] introduces a matching index considering the temporal correlation, overall distribution, and dynamic characteristics of net load and BESSs, aiming for the collaborative optimal dispatch of FRs. Similarly, [18] explores the rationality of typical FR modeling and dispatch schemes, investigating the reasonable arrangement of unit output within FR participation contexts. While these dispatch schemes can form relatively controllable unit combinations, the features of research elements involved in coordinating the optimal operation of multi-type FRs remain heterogeneous, posing a challenge in quantifying the regulated capability difference among them.

Diversified FRs exhibit distinct fundamental features concerning response power, energy, direction, and cost. Furthermore, their technical and economic benefits for the power grid, when matching with PEBD, vary considerably. In a bi-level wind power capacity optimization planning model [19], a dynamic source-load tracking coefficient is proposed at the operation level, which reflects the matching degree between the fluctuating wind power and the controllable hydroelectric power. Reference [20] establishes a renewable energy output tracking control algorithm based on a state-queuing model, aiming to minimize tracking errors, quantified as the sum of squares of differences between renewable energy output and load power. Reference [21] presents an interactive decision model for source-load matching, integrating day-ahead and real-time scheduling. Additionally, [22] proposes a source-load value matching method considering numerous uncertain factors, calculating matching degrees to effectively align source and load values. Reference [23] establishes a function model for volatility-based smoothing coefficients and source-load timing matching coefficients to enhance the timing matching degree between wind power output and grid load, thereby mitigating the adverse impact of wind power connection on the power system. Moreover, [24] proposes a model considering the comprehensive Spearman constant and Euclidean distance matching indices to reduce energy consumption costs for each community under the guidance of matching index. While these studies aim to incorporate the matching degree into optimized FR operation to reduce power deviation between source output and load power, they often lack a comprehensive depiction for the features of multi-type FRs. Additionally, they primarily focus on the matching degree between sources and loads from the perspective of partial power matching, making it challenging to fully capture the differentiated regulation capabilities of multi-type FRs for different PEBDs.

Given the aforementioned limitations in previous studies, which primarily focus on allocating predetermined types of BESSs and characterizing FR features solely from the perspective of power and energy, addressing cost issues caused by imbalance power becomes challenging. Consequently, to effectively quantify feature differences among multi-type FRs and coordinate the operating performance and economic benefits of the power grid, we propose an optimal planning and operation method based on a differentiated feature matching method between FRs and PEBD. The main contributions of this study are summarized as follows.

1) The establishment of an optimized planning model for diversified ESs, including BESSs, to achieve optimal deployment of ES types, node locations, rated power, and rated capacities. This model effectively leverages BESSs to reduce comprehensive operating costs and alleviate imbalance power in the power grid.

2) The development of an optimal operation algorithm for multi-type FRs based on a differentiated feature matching method. This algorithm outputs the response sequence of FRs, characterizing the feature matching process between FRs and PEBD through difference quantification and mapping relationships. Moreover, this algorithm deconstructs the optimization and decision-making process for multi-type FRs, ensuring they meet PEBD requirements while economically reducing imbalance power in the power grid.

3) The validation of the feasibility and effectiveness of the proposed optimal planning and operation method using actual data from FRs in northwest China.

The remainder of this paper is organized as follows. In Section II, detailed considerations of the optimal planning for diversified ESs containing BESSs are analyzed and modeled. Section III presents the framework of the optimal planning and operation method based on differentiated feature matching method for multi-type FRs, outlining the main objectives and constraints of the optimization algorithm. Section IV presents the results and discussion based on case studies. The conclusion and future work are given in Section V.

II. Analysis and Modeling of Optimal Planning for Diversified ESs

A. Modeling of Diversified ESs

As a key FR to satisfy PEBD, the optimal planning of ES types is closely tied to the operating performance of power grids. Diversified ESs differ in their regulation capabilities. Therefore, achieving a reasonable allocation of diversified ESs is a pivotal challenge among the diverse ES types, which include widely applicable BESSs. Ensuring the stable operation of the power grid and substantially enhancing its economic benefits hinge upon the reasonable planning of ESs.

Li-B is a typical representation of BESSs, known for its lower capital cost, stable operation, and flexible response range, allowing it to adapt to various demands. Compressed air energy storage (CAES) offers advantages such as larger ES capacity and extended operational lifespan. Pumped hydroelectric storage (PHS) stands out with its substantial ES capacity, extended operational lifespan, and shorter response time. Supercapacitor energy storage (SCES) is characterized by its higher power density, and rapid charging and discharging capability. To highlight the different regulation capabilities of diversified ESs, a resource repository of diversified ESs K containing Li-B, CAES, PHS, and SCES is constructed for optimal planning, as shown in (1), and the comparison of differentiated regulation capabilities of the four types of ESs is shown in Fig. 1 [25], [26].

$$K=\{\mathrm{Li}, \mathrm{Ca}, \mathrm{Ps}, \mathrm{Sc}\} \tag{1}$$

where Li, Ca, Ps, and Sc represent the Li-B, CAES, PHS, and SCES, respectively.

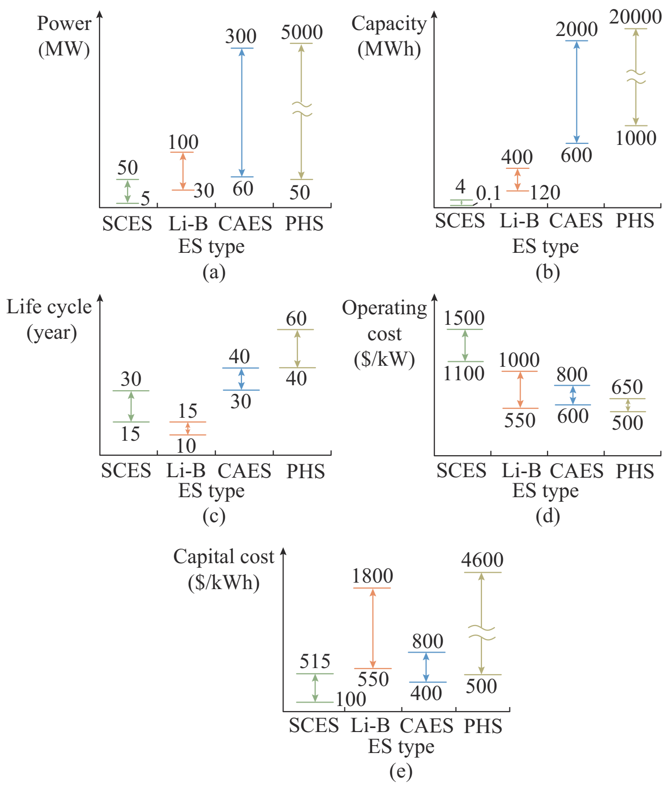

Fig. 1. Differentiated regulation capabilities of diversified ESs. (a) Power range. (b) Capacity range. (c) Life cycle range. (d) Operating cost range. (e) Capital cost range.

The model constructed by diversified ESs is as follows:

$$E_k(t)=E_k(t-1)+\tau_{ES,k}\int_{t-1}^{t} P_{ES,k}(\tau)\mathrm{d}\tau \quad k\in K \tag{2}$$

where $E_k(t)$ and $E_k(t-1)$ are the capacities of ES k at time t and $t-1$, respectively; $\tau_{ES,k}$ is the charging and discharging coefficient of ES k; and $P_{ES,k}(\tau)$ is the operating power of ES k at time τ.

The cost of ES is categorized into capital cost and operating cost. Specifically, considering the life cycle and investment recovery coefficient, the capital cost is equivalent to the initial investment cost, which is apportioned as the daily depreciation cost of ES, represented as follows:

$$R_k=\frac{r(1+r)^{T_k}}{(1+r)^{T_k}-1} \quad k\in K \tag{3}$$

$$C_{inv}=\frac{1}{365}\sum_{k\in K} R_k c_{E,k} E_{N,k} \tag{4}$$

where R_k is the annual investment recovery coefficient of ES k; C_{inv} is the daily depreciation cost of ES; T_k is the life cycle of ES k; r is the discount rate; $c_{E,k}$ is the unit capital cost of life cycle of ES k; and $E_{N,k}$ is the rated capacity of ES k.

The operating cost of diversified ESs C_{op} is as follows:

$$C_{op}=\sum_{k\in K} c_{op,k}\left|P_{ES,k}\right| \tag{5}$$

where $c_{op,k}$ is the unit operating cost of ES k; and $P_{ES,k}$ is the operating power of ES k.

B. Planning Model of Diversified ESs

The four types of ESs differ in regulation capabilities such as rated power, life cycle, operating cost, and capital cost, as illustrated in Fig. 1. In regional power grids, diversified ESs are strategically allocated to attain varied technical and economic benefits for power grid regulation. Consequently, leveraging the differentiated regulation capabilities of diversified ESs, an optimal planning model of ESs from K is formulated. This model serves as a prerequisite for implementing the differentiated feature matching method of FRs to meet the PEBD within the power grid.

1) ES Planning Constraints

The rated power of ES k satisfies a certain power range, as shown in Fig. 1(a). A 0-1 decision variable $\lambda_{k,l}$ is introduced to depict the planning state of ES k at node l and to realize the planning of diversified ESs, which is shown as follows:

$$P_{ES,k,\min}\le\lambda_{k,l}P_{ES,k,N}\le P_{ES,k,\max} \quad k\in K \tag{6}$$

where $P_{ES,k,N}$ is the rated power of ES k; $P_{ES,k,\min}$ and $P_{ES,k,\max}$ are the minimum and maximum rated power of ES k, respectively; and $\lambda_{k,l}=1$ and $\lambda_{k,l}=0$ represent that ES k is allocated at node l or not, respectively.

Formula (6) is nonlinear due to the multiplication of a 0-1 state variable with a continuous variable, which can be linearized by the big-M method as:

$$P_{N,k}=\lambda_{k,l}P_{ES,k,N} \quad k\in K \tag{7}$$

$$P_{N,k}\le P_{ES,k,N} \quad k\in K \tag{8}$$

$$P_{N,k}\le P_{ES,k,N}-M(1-\lambda_{k,l}) \quad k\in K \tag{9}$$

$$\lambda_{k,l}P_{ES,k,\min}\le P_{N,k}\le\lambda_{k,l}P_{ES,k,\max} \quad k\in K \tag{10}$$

where $P_{N,k}$ is the introduced intermediate variable; and M is an infinite number.

Meanwhile, the optimal planning of diversified ESs also satisfies the following constraints:

$$\sum_{k\in K}\lambda_{k,l}\le 1 \tag{11}$$

$$\sum_{k\in K}\sum_{l}\lambda_{k,l}\le N_{ES,\max} \tag{12}$$

$$-\tau_{ES,k}P_{ES,k,N}\le P_{ES,k}\le\tau_{ES,k}P_{ES,k,N} \quad k\in K \tag{13}$$

$$E_{ES,k,N}=\psi_k P_{ES,k,N} \quad k\in K \tag{14}$$

where $N_{ES,\max}$ is the maximum number of allocated ESs in the regional power grid; $E_{ES,k,N}$ is the rated capacity of ES k; and ψ_k is the energy multiplication coefficient of ES k. Constraint (11) restricts the amount of allocated ESs at any node. Constraint (12) limits the total amount of allocated ESs. Constraint (13) ensures that the operating power of ESs remains within their rated power limits. Constraint (14) establishes the relationship between the rated power and rated capacity of ESs.

2) Power Flow Constraints

$$P_{ij}=(\theta_i-\theta_j)/X_{ij} \tag{15}$$

$$-P_{ij,\max}\leq P_{ij}\leq P_{ij,\max} \tag{16}$$

where P_{ij} is the active power flow from nodes i to j; θ_i and θ_j are the phase angles of the voltages at nodes i and j, respectively; X_{ij} is the reactance from nodes i to j; and $P_{ij,\max}$ is the maximum value of the line power flow from nodes i to j.

3) Power Balance Constraints

$$\sum_i P_{Th,i}+P_{Hy}+P_{ES,k}+P_{Ti}+P_{Cl}=P_{ij}+P_{base}+\Delta P_{Ld} \tag{17}$$

$$\Delta P_{Ld}=\Delta P_{tr}+\Delta P_{re}+\Delta P_{ad} \tag{18}$$

where $P_{Th,i}$ is the output of thermal power unit i; P_{Hy} is the output of hydroelectric power unit; P_{Ti} is the tie-line power, representing the net power exchange between the power grid and external grid; P_{Cl} is the clean energy power of a typical day; P_{base} is the base load power; ΔP_{Ld} is the power of flexible loads, which include transferable loads (TLs), reducible loads (RLs), and adjustable loads (ALs); ΔP_{tr} is the power of TLs, maintaining their electricity consumption constant during the regulated cycle; ΔP_{re} is the power of RLs, which can be partially or completely reduced for loads with low reliable requirements; and ΔP_{ad} is the power of ALs besides TLs and RLs.

4) Thermal Power Unit Constraint

$$\mu_{Th,i}P_{Th,i,N}\leq P_{Th,i}\leq P_{Th,i,N} \tag{19}$$

where $\mu_{Th,i}$ is the minimum technical output coefficient; and $P_{Th,i,N}$ is the rated power of thermal power unit i.

5) Hydroelectric Power Constraint

$$0\leq P_{Hy}\leq P_{Hy,N} \tag{20}$$

where $P_{Hy,N}$ is the rated power of hydroelectric power unit.

6) Tie-line Constraint

$$\left|P_{Ti}\right|\leq P_{Ti,\max} \tag{21}$$

where $P_{Ti,\max}$ is the maximum value of tie-line power.

7) Flexible Load Constraints

$$\alpha_{\min}P_{tr}\leq \Delta P_{tr}\leq \alpha_{\max}P_{tr} \tag{22}$$

$$\beta P_{re}\leq \Delta P_{re}\leq P_{re} \tag{23}$$

$$\gamma_{\min}P_{ad}\leq \Delta P_{ad}\leq \gamma_{\max}P_{ad} \tag{24}$$

where $\alpha_{\min}$ and $\alpha_{\max}$ are the lower and upper regulated coefficients for TLs, respectively; P_{tr} is the planned power consumption of TLs; P_{re} is the planned power consumption of RLs; P_{ad} is the planned power consumption of ALs; β is the regulated coefficient for RLs; and $\gamma_{\min}$ and $\gamma_{\max}$ are the lower and upper regulated coefficients for ALs, respectively.

8) Objective Function

In this paper, the comprehensive cost of power grid F is considered as the optimal objective, including generation cost and carbon emission penalty cost F_{Gen}, tie-line cost F_{Ti}, flexible load cost F_{Ld}, and cost of diversified ESs F_{ES}. It is expressed as:

$$\min F=F_{Gen}+F_{Ti}+F_{Ld}+F_{ES} \tag{25}$$

$$\begin{cases} F_{Gen}=P_{Th,i}(c_{Th}+c_{Ca})+P_{Hy}c_{Hy} \\ F_{Ti}=\left|P_{Ti}\right|c_{Ti} \\ F_{Ld}=\left|\Delta P_{Ld}\right|c_{Ld} \\ F_{ES}=C_{inv}+C_{op} \end{cases} \tag{26}$$

where c_{Th} and c_{Ca} are the unit generation cost and carbon emission penalty cost of thermal power units, respectively; c_{Hy} is the unit generation cost of hydroelectric power unit; c_{Ti} is the unit cost of tie-line power; and c_{Ld} is the unit regulated cost of flexible loads.

III. Framework of Optimal Planning and Operation Method Based on Differentiated Feature Matching for Multi-type FRs

The block diagram of the proposed method for multi-type FRs based on differentiated feature matching is illustrated in Fig. 2. First, a planning model of FRs is established, as detailed in Section II, to identify the type and parameter of multi-type FRs including BESSs. This enables the optimized planning of ES types, node locations, rated power, and rated capacity by mixed-integer linear programming (MILP). Subsequently, the feature matrices of FRs and PEBD in the power grid are constructed, and the feature difference including response potential, response direction, and response cost is quantified using the Euclidean distance metric. Following this, a matching degree is proposed to characterize matching priority of FRs, and a mapping relationship is proposed to analyze the matching process between FRs and PEBD. Finally, considering the regulated boundary of multi-type FRs and utilizing the aforementioned normalized feature difference as the objective function, the optimal operation algorithm of FRs iterates with feature matching framework to output the response sequence of FRs.

A. Differentiated Feature of FRs

1) Feature Set of FRs

In this paper, the FRs in the power grid are considered to include thermal power units, hydroelectric power units, tie-lines, TLs, RLs, ALs, and allocated ESs. A feature set of FRs is constructed by refining the response potential, response direction, and response cost of FRs. The set consisting of these FRs is:

$$U=\{u_m|u_{Th},u_{Hy},u_{Ti},u_{tr},u_{re},u_{ad},u_{ES}\} \tag{27}$$

where u_{Th}, u_{Hy}, u_{Ti}, u_{tr}, u_{re}, u_{ad}, and u_{ES} represents the thermal power unit, hydroelectric power unit, tie-line, TL, RL, AL, and allocated ES, respectively; and u_m represents any FR in set U.

The main influencing factors of the response potential include the down-regulation and up-regulation capabilities. The response potential of FRs can be expressed as:

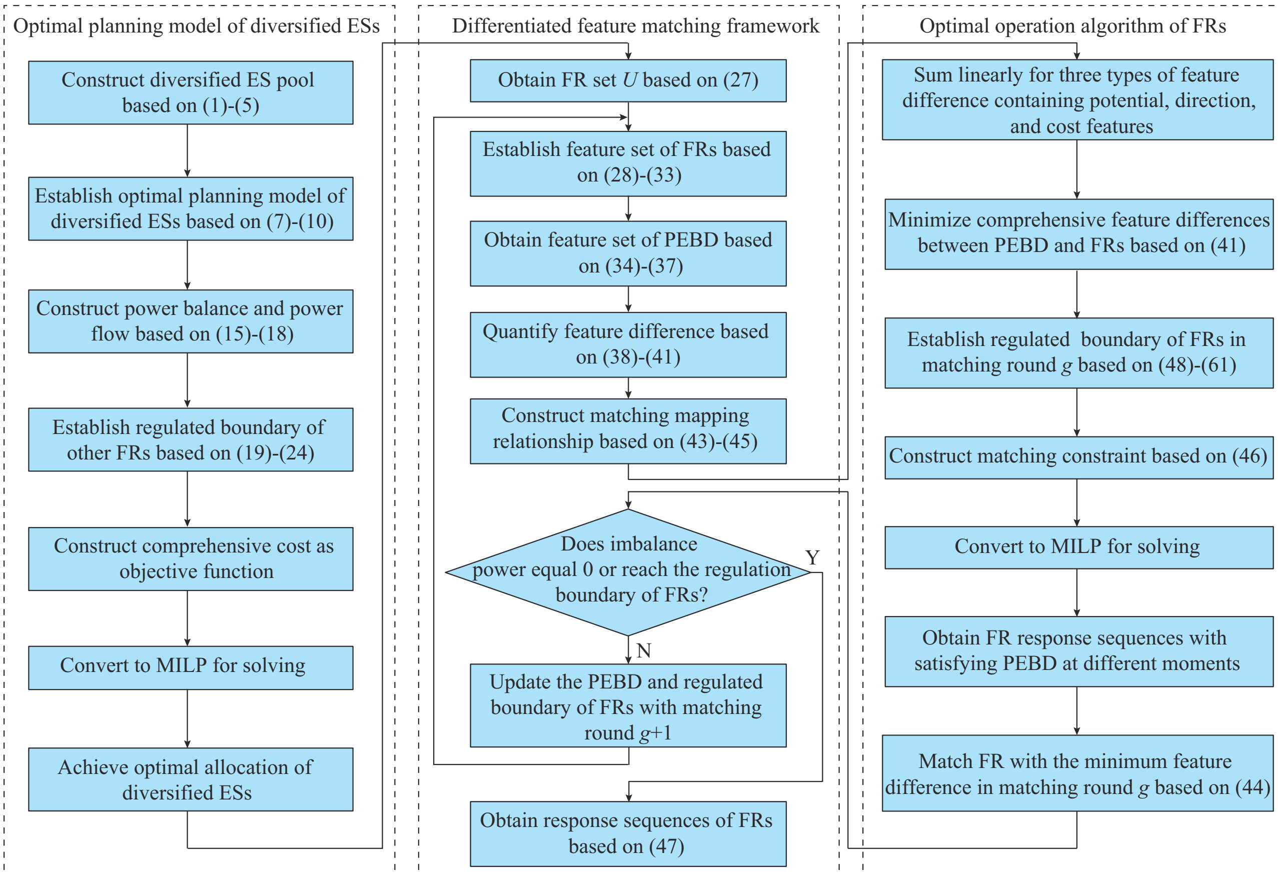

Fig. 2. Block diagram of proposed method for multi-type FRs.

$$Q_m=(P_m(t)-P_{m,\min})(P_{m,\max}-P_m(t)) \quad m\in U \tag{28}$$

where m is the element of FR set U; Q_m is the response potential of FRs; $P_m(t)$ is the response power of FRs at time t; and $P_{m,\min}$ and $P_{m,\max}$ are the minimum and maximum power of FRs, respectively.

Since (28) is nonlinear and difficult to solve directly, this paper employs the segmented linearization method mentioned in [27] to transform the quadratic function into a segmented linear function with b segments. Thus, (28) can rewritten as:

$$Q_m=\sum_{s=1}^{b} Y_{m,s}\,p_{m,t,s}+H \tag{29}$$

where $Y_{m,s}$ is the slope of each function segment after segment linearization; $p_{m,t,s}$ is the segmented response power of FRs; and H is the response potential of the minimum response power.

Meanwhile, $p_{m,t,s}$ and H satisfy:

$$\begin{cases} H=-P_{\min}^2+(P_{m,\min}+P_{m,\max})P_{\min}-P_{\min}P_{\max} \\ 0\le p_{m,t,s}\le (P_{\max}-P_{\min})/b \\ P_m(t)=\displaystyle\sum_{s=1}^{b} p_{m,t,s}+P_{\min} \end{cases} \tag{30}$$

where $P_{\min}$ and $P_{\max}$ are the minimum and maximum segment values of $P_m(t)$, respectively.

The response direction of FRs R_m represents the change trend of response power at next moment relative to current moment, which can be calculated as:

$$R_m=(P_m(t+1)-P_m(t))/T \quad m\in U, t=1,2,...,T-1 \tag{31}$$

where T is the regulated cycle.

The response costs of FRs C_m primarily consist of response power and unit response cost, which can be calculated as:

$$C_m=c_m\left|P_m(t)\right| \quad m\in U \tag{32}$$

where c_m is the unit response cost of FRs.

Based on the proposed feature of FRs, the feature set of FRs is:

$$\delta_m=\{Q_m, C_m, R_m\} \tag{33}$$

2) Feature Set of PEBD

PEBD is the regulated demand caused by power mismatching between generation and load of regional power grid, which can be calculated as:

$$P_{PEBD,0}(t)=P_{load}(t)-P_{PV}(t)-P_{wind}(t)-\sum_i \mu_{Th,i}P_{Th,i,N} \tag{34}$$

where $P_{PEBD,0}(t)$ is the initial PEBD at time t in the power grid; $P_{load}(t)$ is the forecasted load power; $P_{PV}(t)$ is the forecasted photovoltaic (PV) power; and $P_{wind}(t)$ is the forecasted wind power.

The set of PEBD is as follows:

$$V=\{v_1, v_2, ...v_t, ..., v_T\} \tag{35}$$

where v_t is the PEBD at time t, and its value is equal to $P_{PEBD,0}(t)$.

Corresponding to the features of FRs, the generalized features of PEBD are refined into power demand, direction demand, and cost demand. The feature set of PEBD can be expressed as:

$$\vartheta_t = \{Q_t, R_t, C_t\} \tag{36}$$

where Q_t is the power demand of PEBD; R_t is the direction demand of PEBD; and C_t is the cost demand of PEBD.

$$\begin{cases} Q_t = P_{PEBD,g}(t+1) \\ R_t = (P_{PEBD,g}(t+1) - P_{PEBD,g}(t))/T \\ C_t = c_{PEBD}\left| P_{PEBD,g}(t) - P_{im,g}(t) \right| \end{cases} \tag{37}$$

where c_{PEBD} is the unit cost of demand assessment reduction; $P_{PEBD,g}(t)$ is the PEBD at time t in matching round g; and $P_{im,g}(t)$ is the imbalance power after optimal operation, and the value is equal to $P_{PEBD,0}(t)$ when $g=0$.

B. Feature Matching Between FRs and PEBD

The aforementioned three types of features characterize the responsiveness of multi-type FRs. Specifically, the difference between response potential and power demand at the next moment portrays regulated capability fitness of FRs to PEBD, the difference between response direction and direction demand depicts the tracking effect of FRs to PEBD, and the difference between response cost and cost demand portrays PEBD cost of power grid. Accordingly, the feature difference between FRs and PEBD can be quantified as:

$$d_{m,t}(\Lambda) = \sqrt{\sum_{m\in U}\sum_{t=1}^{T}(\delta_m(\Lambda) - \vartheta_t(\Lambda))^2} \tag{38}$$

$$\Lambda = \{Q, R, C\} \tag{39}$$

where $d_{m,t}$ is the feature difference; Λ is generalized feature set of FRs and PEBD; and Q, R, and C are the generalized potential feature, direction feature, and cost feature of FRs and PEBD, respectively.

Feature difference is normalized by the range method, which can be expressed as:

$$d_{m,t,n}(\Lambda) = \frac{d_{m,t}(\Lambda) - \min\{d_{m,t}(\Lambda)\}}{\max\{d_{m,t}(\Lambda)\} - \min\{d_{m,t}(\Lambda)\}} \tag{40}$$

where $d_{m,t,n}$ is the normalized feature difference.

From (38), it can be inferred that a smaller difference between FRs and PEBD results in a higher matching priority. Therefore, this paper defines f to characterize the matching priority of multi-type FRs, which is determined through linear summation as follows:

$$f = \sum_{t=1}^{T}(d_{m,t,n}(Q) + d_{m,t,n}(R) + d_{m,t,n}(C)) \tag{41}$$

where $d_{m,t,n}(Q)$, $d_{m,t,n}(R)$, and $d_{m,t,n}(C)$ are the normalized feature differences of potential, direction, and cost, respectively.

Meanwhile, ρ is introduced to measure the matching degree between FRs and PEBD, which is as follows:

$$\rho = \sqrt{1 - f^x} \tag{42}$$

where x is the matching coefficient.

The set of FRs U and set of PEBD V form the feature space F. This paper defines the mapping function $\mu: U \rightarrow V$ as the matching process between U and V in the feature space F. The influencing factors are manifested in the form of differentiated features in this paper, and the mapping function satisfies the following condition: for any element in V, there always exists an element in U to match it, which is expressed as:

$$\forall v_t \in V: \exists \mu(u_m) \in v_t, m \geq 0 \tag{43}$$

where $\mu(u_m) \in v_t$ is the matching pair composed by u_m and v_t.

Different response sequences of FRs represent different regulation strategies, and different moments of PEBD are matched with different sequences of FRs to ensure the balance between the supply of FRs and the PEBD in terms of response potential, response direction, and response cost.

$$\| d \|_\infty = \min_{1\leq m\leq M}(d_{m,t,n}(\Lambda)) \tag{44}$$

where d is the minimum value of feature difference.

When (43) and (44) are satisfied, FR m prioritizes to match with PEBD in matching round $g=1$. And PEBD is continuously updated in the subsequent matching round $g+1$, resulting in the response sequence of FRs being output under dynamic PEBD.

On this basis, a 0-1 state variable that characterizes whether the FR constitutes a matching pair with PEBD being introduced as:

$$\chi_{mt} = \begin{cases} 1 & \mu(u_m) \in v_t \\ 0 & \mu(u_m) \notin v_t \end{cases} \tag{45}$$

As the matched FR reduces PEBD by a certain power after matching round g, the PEBD will be corrected in next matching round:

$$P_{PEBD,g+1}(t) = P_{PEBD,g}(t) - P_{m,g}(t) \quad g \geq 0 \tag{46}$$

where $P_{PEBD,g}(t)$ is the power of PEBD at moment t in matching round g; and $P_{m,g}(t)$ is the matched FR in matching round g.

Finally, until the PEBD is 0 or the FR regulation boundary is reached, the stable set of response sequences for FRs is output, which can be expressed as:

$$\boldsymbol{V}_{1\times T} = \boldsymbol{U}_{1\times m}\boldsymbol{\chi}_{m\times T} \tag{47}$$

where $\boldsymbol{V}_{1\times T}$ is the matrix of PEBD in period T; $\boldsymbol{U}_{1\times m}$ is the matrix of m types of FRs; and $\boldsymbol{\chi}_{m\times T}$ is the matching state matrix of FR and PEBD.

C. Optimal Operation Algorithm of FRs

1) Objective Function

In this paper, the objective of power grid operation is to minimize the comprehensive feature differences of three aspects: response potential–power demand, response direction–direction demand, and response cost–cost demand. Accordingly, the objective function is shown in (41).

2) Power Flow Constraints

$$P_{ij,g}(t) = (\theta_i - \theta_j)/X_{ij} \tag{48}$$

$$-P_{ij,\max} \leq P_{ij,g}(t) \leq P_{ij,\max} \tag{49}$$

where $P_{ij,g}(t)$ is the active power flow of the line from node i to node j at time t in matching round g.

3) Power Balance Constraints

$$\sum_i P_{Th,i,g}(t)+P_{Hy,g}(t)+P_{ES,k,g}(t)+P_{Ti,g}(t)=P_{ij,g}(t)+\Delta P_{tr,g}(t)+\Delta P_{re,g}(t)+\Delta P_{ad,g}(t)+P_{PEBD,g}(t) \tag{50}$$

where $P_{Th,i,g}(t)$ is the power of thermal power unit i in matching round g; $P_{Hy,g}(t)$ is the output of hydroelectric power unit in matching round g; $P_{ES,k,g}(t)$ is the response power of ES k in matching round g; $P_{Ti,g}(t)$ is the tie-line power in matching round g; and $\Delta P_{tr,g}(t)$, $\Delta P_{re,g}(t)$, and $\Delta P_{ad,g}(t)$ are the response power of TLs, RLs, and ALs in matching round g, respectively.

4) Conventional Resource Constraints

$$0 \le \sum_g P_{Th,i,g}(t) \le (1-\mu_{Th,i})P_{Th,i,N} \tag{51}$$

$$0 \le \sum_g P_{Hy,g}(t) \le P_{Hy,N} \tag{52}$$

$$\sum_g \left| P_{Ti,g}(t) \right| \le P_{Ti,\max} \tag{53}$$

5) Flexible Load Constraints

TLs are required to keep the power consumption constant during the regulated cycle and satisfy certain response range constraints, which are expressed as:

$$\sum_t \Delta P_{tr,g}(t)=0 \tag{54}$$

$$\alpha_{\min} P_{tr}(t) \le \sum_g \Delta P_{tr,g}(t) \le \alpha_{\max} P_{tr}(t) \tag{55}$$

Constraints must be satisfied to ensure that RLs adhere to certain response range and number of reduced regulation times, thus avoiding the impact of power utilization. These constraints are expressed as:

$$r_t \beta P_{re}(t) \le \sum_g \Delta P_{re,g}(t) \le P_{re}(t) \tag{56}$$

$$\sum_{t=1}^{T} r_t \le N_{\max} \tag{57}$$

where r_t is number of the reduced regulation times of RLs during regulated cycle; and $N_{\max}$ is the upper limit of the number of reduced regulation times.

Certain response range constraint should be satisfied by ALs, which is expressed as:

$$\gamma_{\min} P_{ad}(t) \le \sum_g \Delta P_{ad,g}(t) \le \gamma_{\max} P_{ad}(t) \tag{58}$$

6) ES Constraints

$$-\tau_{ES,k} P_{ES,k,N} \le \sum_g P_{ES,k,g}(t) \le \tau_{ES,k} P_{ES,k,N} \tag{59}$$

$$\sum_{t=1}^{T} P_{ES,k,g}(t)=0 \tag{60}$$

$$0 \le E_{ES,k,0} + \sum_{t'}\sum_g P_{ES,k,g}(t')\Delta t \le E_{ES,k,N} \quad t' \in [0,t] \tag{61}$$

where $E_{ES,k,0}$ is the initial capacity of allocated ES k.

7) Matching Constraints

The feature matching constraints are shown in (30) and (46).

IV. Case Study

A. Case Description

To demonstrate the feasibility and effectiveness of proposed method, case studies are conducted using an actual 25-bus regional power grid in northwest China, as shown in Fig. 3. The MILP algorithm is implemented using MATLAB 2021.

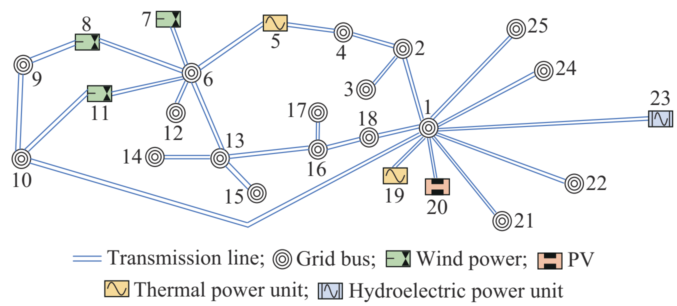

Fig. 3. An actual 25-bus regional power grid in northwest China.

The technology parameters of the regional power grid are displayed in Table I, and the basic technology parameters of diversified ESs are provided in Table II [28], where SOC denotes for state of charge. The data in a typical day are obtained by clustering one year's power generation and load data in the ES planning model, and several cases are conducted as follows.

TABLE I
TECHNOLOGY PARAMETERS OF REGIONAL POWER GRID

Type	Rated value (MW)	The minimum value (MW)
Thermal power	4697.0	2348.5
Hydroelectric power	476.0	0
Wind power	5950.0	
PV power	4410.0	
Tie-line power	800.0	–800
Forecasting load	16509.0	
TL	4592.0	2188
RL	2344.2	$0.7P_{re}(t)$
AL	847.9	$0.7P_{ad}(t)$

TABLE II
TECHNOLOGY PARAMETERS OF DIVERSIFIED ESs

ES type	$P_{ES,k,\min}$ (MW)	$P_{ES,k,\max}$ (MW)	Life cycle (year)	Initial SOC	Discount rate (%)	ψ_k
Li-B	300.00	100	10	0.5	6.70	4.0
CAES	100.00	1000	30	0.5	6.70	10.0
PHS	0.01	1	30	0.5	6.70	0.1
SCES	200.00	2000	50	0.5	6.70	20.0

Case 1: the net load of the regional power grid is simulated, and the results are shown in Fig. 4.

Case 2: FRs except for ESs participate in the regional power grid regulation without considering the proposed method.

Case 3: based on Case 2, the PHS participates in the optimal planning and the differentiated regulation capabilities of ESs are ignored.

Case 4: based on Case 2, diversified ESs participate in the optimal planning considering differentiated regulation capabilities, and the feature matching is ignored in the optimal operation of FRs.

Case 5: based on Case 4, multi-type FRs participate in the regional power grid regulation through the proposed method considering feature matching.

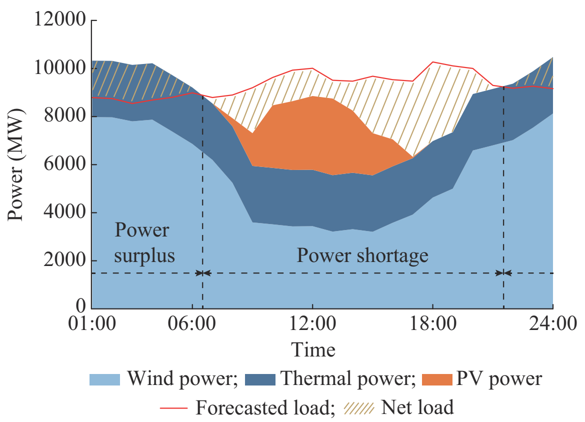

Fig. 4. Net load results of regional power grid.

B. Power Grid Regulation Analysis Using Optimal Planning of Diversified ESs

Based on (32), the value of PEBD equals the net load of the regional power grid, which is shown in Fig. 4. Specially, the regional power grid experiences a power shortage during the period from 07:00 to 21:00, and power surplus occurs during other periods. Based on the regulation demand in Case 1 and the established planning model of ESs in Section II, specific planning results of diversified ESs in Cases 3 and 4 are presented in Table III. In Case 3, the PHS is allocated to nodes 2 and 10 with respective rated power of 200 MW and 695 MW. The optimal planning result in Case 4 reveals that the allocated ES types are Li-B, PHS, and CAES, with respective rated power of 148 MW, 200 MW, and 540 MW. Li-B is allocated to most nodes because it has more flexible response capacity and lower capital cost. Notably, the total rated power of Case 3 and Case 4 is 895 MW and 885 MW, respectively. This variance can be attributed to the fact that a single ES type with limited regulation capacity in Case 3 faces challenges in achieving the coordinated complementary advantages of diversified ESs. Consequently, it is necessary to further increase the allocated capacity to satisfy the PEBD.

To validate the effectiveness of proposed optimal planning model, the technical and economic benefits of the allocated ESs in Case 3 and Case 4 are compared. In both Case 3 and Case 4, the operating power and the SOC of the allocated ESs are shown in Fig. 5.

It can be observed that the charging and discharging periods closely align with the power shortage and power surplus periods shown in Fig. 4. During power surplus periods, the allocated ESs are charged to accommodate surplus power within the power grid, gradually increasing their SOC. Conversely, during power shortage periods, the ESs are discharged to supplement the power shortage, gradually reducing their SOC. It is worth noting that the SOC of the ESs is maintained constant at the beginning and end of the regulation cycle, as indicated by (54).

TABLE III
OPTIMAL PLANNING RESULTS OF DIVERSIFIED ESs IN CASES 3 AND 4

Case	ES type	Node	Rated power (MW)	Rated capacity (MWh)
Case 3	PHS	2	200	4000
	PHS	10	695	13900
Case 4	Li-B	4	60	240
	PHS	11	200	4000
	CAES	20	540	5400
	Li-B	24	88	352

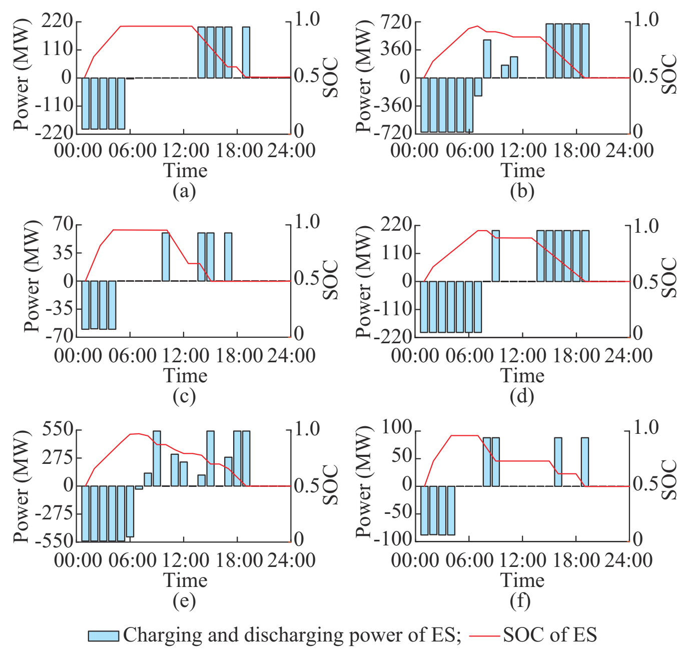

Fig. 5. Operating power and SOC of allocated ESs in Cases 3 and 4. (a) PHS at node 2 in Case 3. (b) PHS at node 10 in Case 3. (c) Li-B at node 4 in Case 4. (d) PHS in Case 4. (e) CAES in Case 4. (f) Li-B at node 24 in Case 4.

From Fig. 5(a) and (b), it is evident that the operating power of PHSs allocated at nodes 2 and 10 in Case 3 exhibits no significant differences in response frequency and direction. This phenomenon arises because the allocated PHS units differ only in their ES capacities, and the PHS with higher rated power at node 10 primarily satisfies the PEBD. However, as shown in Fig. 5(c)-(f), it is apparent that the Li-Bs allocated at nodes 4 and 24 in Case 4 undergo only 8 charging and discharging cycles, significantly fewer than those of CAES and PHS. This notable discrepancy can be primarily attributed to the higher charging and discharging costs of Li-Bs, as indicated in Fig. 1. Consequently, Li-B has the advantage of capacity allocation compared with CAES and PHS, while CAES and PHS have priority for participation in ES operation due to their lower operating costs and higher regulation capacities.

The coordinated optimization between diversified ESs and other FRs plays a vital role in satisfying PEBD and enhancing the economic benefits of the regional power grid. The optimal operating results of multi-type FRs in different cases considering allocated ESs are illustrated in Fig. 6.

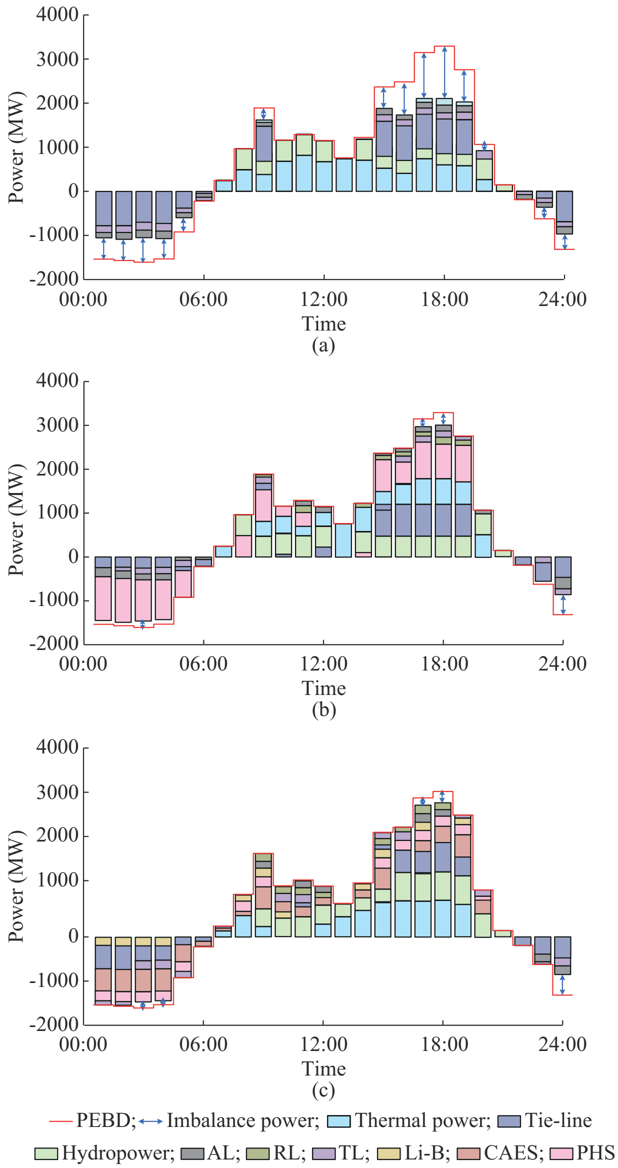

Fig. 6. Optimal operating results of multi-type FRs in different cases considering allocated ESs. (a) Case 2. (b) Case 3. (c) Case 4.

The regulation mechanism for FRs participating in the regulation of regional power grid in Case 2 is outlined as follows. During power shortage periods, the power generation and tie-line supply are increased, while the power demand from the load is reduced, thereby the power shortage is supplemented to maintain the power balance of the regional power grid. Conversely, during power surplus periods, the power supply is reduced, and the load power as well as the power output from tie-line is increased, thus the power surplus of the regional power grid is effectively accommodated. Based on the regulation mechanism in Case 2, the regulation mechanism of multi-type FRs, which aims to ensure the power balance of power grid, is as follows: the ES is discharged during power shortage periods, and it is charged during power surplus periods.

To underscore the superiority of the planning model of diversified ESs, a comparative technical and economic analysis of Cases 2-4 is performed. In terms of technical analysis, the reduction proportion in net load across each case is compared. In Case 1, 78.65% of the net load is accommodated through conventional regulation resources and flexible loads to satisfy certain PEBD. However, there remains a net load that cannot be accommodated at 14 regulation moments, occuring at 01:00-05:00, 09:00, 15:00-20:00, and 23:00-24:00. Leveraging the advantages of ESs compared with other FRs in terms of regulated power, capacity, and cost, 97.32% of the net load is accommodated in Case 3. In Case 4, 97.46% of the net load is accommodated through the coordinated complementary of diversified ESs, resulting in an undissipated energy deficit of only 849.5 MWh.

Regarding economic analysis, the comprehensive costs gradually decrease from Case 2 to Case 4, as depicted in Fig. 7. Specifically, the costs of thermal power units and carbon emission penalties also decrease across these cases, indicating that the diversified ESs with differentiated regulation capabilities contribute to reducing the output of thermal power units and carbon emissions, aligning with the goal of achieving the "carbon peak and carbon neutrality". The total cost of ESs in Case 4 (with the costs of Li-B, SCES, and PHS of \$22300, \$143600, \$80400, respectively) is \$16100 less than that in Case 3 (with the cost of PHS of \$262400), mainly due to the coordinated optimization of diversified ESs in Case 4, particularly BESSs.

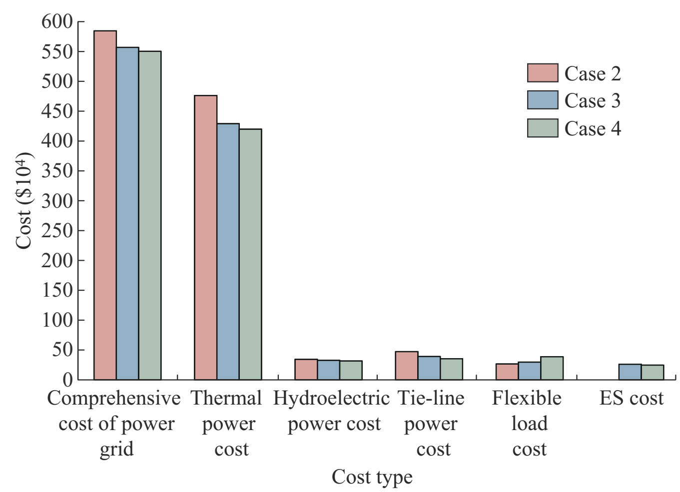

Fig. 7. Comparative costs of FRs in Cases 2-4.

The comparative technical and economic analysis highlights the effectiveness of the optimal planning model for FRs in power grids. Specifically, the optimal planning model of diversified ESs, considering differentiated regulation capabilities, not only decreases imbalance power with less allocated capacity of ESs but also satisfies the PEBD with lower comprehensive costs, consequently reducing the operating cost of allocated ESs.

C. Power Grid Regulation Analysis Using Differentiated Feature Matching Method of Multi-type FRs

To demonstrate the effectiveness of the proposed method, an initial feature matching matrix is established to depict the matching potential of FRs in satisfying PEBD before optimization. The allocated ESs are determined based on the optimization results in Case 4 from Table III. The initial feature matching is defined as follows: the adjustment capacity, rated power, and unit operating cost of FRs are considered as the initial response potential feature, response direction feature, and response cost feature, respectively. By substituting (34) into (37), the initial matrix of PEBD is obtained. Then, the initial feature matching degree between FRs and PEBD is calculated by (38)-(41), serving as a reference for the subsequent analysis of response sequence, as shown in Fig. 8, where Th, Hy, and Ti represent the thermal power unit, hydroelectric power unit, and tie-line, respectively.

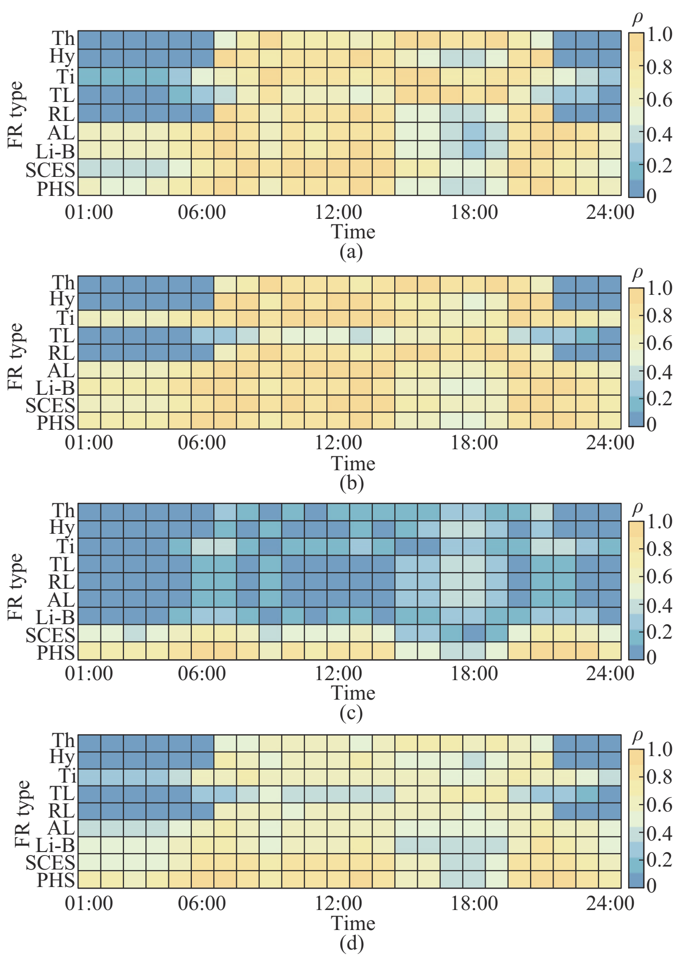

Fig. 8. Initial matching degree between FRs and PEBD. (a) Initial matching degree of response potential. (b) Initial matching degree of response direction. (c) Initial matching degree of response cost. (d) Comprehensive initial matching degree between FRs and PEBD.

As observed from Fig. 8(a)-(c), it is apparent that the adjustable boundaries of multi-type FRs to PEBD are closer and their operating costs are lower, resulting in a higher initial matching degree. The primary reason lies in the fact that FRs with higher regulation capacity can more precisely and effectively satisfy the PEBD of power grid. Moreover, FRs with lower operating costs contribute to enhancing the economic benefits of power grid. After normalizing and linearly weighting the technical and economic features mentioned above, the comprehensive initial matching degree is calculated, as shown in Fig. 8(d). Taking 18: 00 as an example, which is the moment with the highest regulation capacity as depicted in Fig. 6, the matching degree of thermal power units with higher costs is higher compared with other FRs. This is primarily because thermal power units with higher regulation capacity contribute significantly to satisfying PEBD.

Utilizing the proposed method, the optimized operation of multi-type FRs in Case 5 is achieved within the power grid, as illustrated in Fig. 9. Figure 9(a) shows the overall optimization and matching results of multi-type FRs throughout the complete regulated cycle. In particular, typical periods are selected to illustrate the function and significance of three types of feature matching for the optimized operation results in Fig. 9(a). It is worth noting that the typical optimization periods provide a clear illustration based on the main influencing factors.

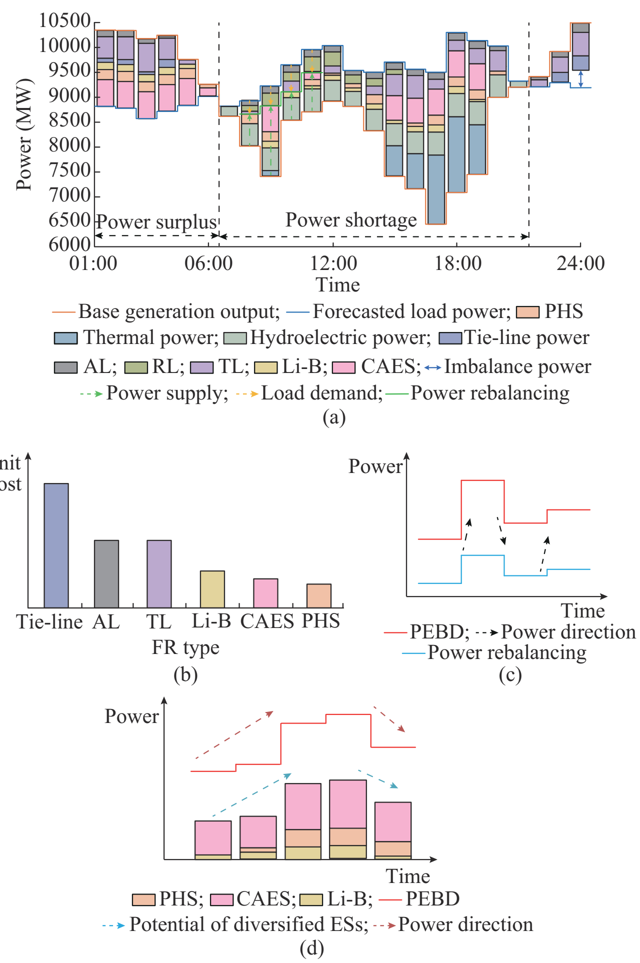

Fig. 9. Optimal operation results of multi-type FRs in Case 5 with proposed method. (a) Matching sequence of multi-type FRs. (b) Cost matching. (c) Direction matching. (d) Potential matching.

First, during the power surplus period from 01:00 to 05:00, as an illustrative example for cost matching analysis, multi-type FRs, including the tie-line, AL, TL, Li-B, CAES, and PHS, actively participate in power regulation to match PEBD. Notably, CAES and PHS are prioritized during this period due to their lower operating costs, as indicated in Fig. 9(b). As a result, CAES and PHS operate with their rated power levels to ensure the power balance of the power grid. In contrast, the tie-line power is minimized to accommodate surplus power due to its highest operating cost.

Furthermore, during the power shortage period from 08:00 to 11:00, as an illustrative example for direction matching analysis, the power shortage is supplemented by increasing the power supply and reducing the load demand. Specially, the power supply is augmented by hydroelectric power, thermal power, Li-B, CAES, and PHS, as indicated by the green dashed arrows in Fig. 9(a). Simultaneously, the AL, RL, and TL reduce the power for load demand, as represented by the yellow dashed arrows in Fig. 9(a). The coordinated effort forms a new power rebalancing curve according to the power supply and load demand, as depicted in Fig. 9(c), which closely follows the direction of the PEBD.

Additionally, during the power shortage period from 15:00 to 19:00, as an illustrative example for the potential matching analysis, the FR with larger response potential is prioritized to match with the higher PEBD. For instance, though the operating cost is higher due to the influence of generation cost and carbon emission penalty cost, thermal power units with wider regulation range can quickly satisfy regulation demand and contribute to reducing the frequent regulation of other FRs with smaller response potential. Similarly, the allocated ESs can track accurately the variation of PEBD based on the great potential of upward and downward regulations. The total discharging power of diversified ESs can track the change trend of PEBD, as shown in Fig. 9(d), and the discharging power trends of Li-B, CAES, and PHS are basically similar with the above total discharging power. In particular, the discharging power of Li-B needs to be comprehensively considered, which is limited by its lower rated power and higher operating cost.

To illustrate the feasibility and effectiveness of the proposed method, a comparative technical and economic analysis of Cases 2-5 is performed, with the results summarized in Table IV.

TABLE IV
TECHNICAL AND ECONOMIC ANALYSIS OF CASES 2-5

Case	The maximum imbalance power (MW)	Net load reduction proportion (%)	Comprehensive cost of power grid ($)	ES cost ($)	Cost of unit PEBD ($/MW)
2	1205.0	78.65	5845600	0	222.14
3	435.4	97.32	5568200	262400	171.00
4	428.2	97.46	5502800	246300	168.75
5	347.2	98.39	5516000	253800	166.65

In terms of technical benefits, the imbalance power of Case 5 is 358.2 MWh, which is 491.3 MWh less than that of Case 4, leading to an increase of net load reduction proportion from 97.46% to 98.39%. Concerning economic benefits, the comprehensive cost of the power grid in Case 5 is $5516000, representing a $13200 increase compared with that of Case 4. Therefore, Case 5 reduces the imbalance power by 491.3 MWh at an additional economic cost of $13200.

To facilitate comparison of unit power regulation costs, the cost of unit PEBD is defined as comprehensive cost divided by total response power of FRs. This metric mainly concentrates on the cost of regulating unit power from the perspective of the power grid regulation department, in contrast to the conventional comprehensive cost. The cost of unit PEBD in Case 5 is reduced by 1.24% compared with that in Case 4. This reduction illustrates that the proposed method can effectively reduce the imbalance power while ensuring economically favorable conditions for the power grid.

The technical and economic analysis comparing Case 4 and Case 5 underscores the effectiveness of the proposed method in harmonizing technical and economic benefits within the power grid. It demonstrates the capability of the proposed method to reduce imbalance power and enhance the utilization of diversified ESs. The prioritization of FRs with superior response potential, response direction, and response cost by the power grid regulation department ensures accurate and efficient satisfaction of PEBD. Conversely, a reduced participation rate in power grid regulation is observed for FRs with lower matching degrees. This preference is attributed to the ability of the proposed method to effectively share feature information between power supply and demand, thereby dynamically tracking the variation of PEBD by considering the multi-dimensional and heterogeneous features of multi-type FRs. Specifically, the iterative calculation of feature differences between multi-type FRs and dynamic PEBD ensures that PEBD consistently matches FRs with minimal differences, effectively decomposing regulated commands. Consequently, the feature differences of multi-type FRs serve as the objective of dynamic iterative optimization for the proposed method, reflecting the power rebalancing process.

V. CONCLUSION

In this paper, we propose and analyze an optimal planning and operation method for multi-type FRs within a regional power grid characterized by a high proportion of clean energy. Recognizing the diverse regulation capabilities of diversified ESs and multi-type FRs in addressing PEBD, we establish an optimal planning model for diversified ESs, including BESSs, and investigate an optimal operation algorithm for multi-type FRs.

1) The established optimal planning model considers the differentiated regulation capabilities of diversified ESs, facilitating the optimal deployment of BESSs. Leveraging the flexible response range and lower capital cost of BESSs, this model effectively reduces imbalance power, ES cost, and comprehensive cost within the power grid.

2) We construct a feature set for multi-type FRs and PEBD, accounting for their inherent heterogeneity. Through difference quantification and mapping relationships, the dif-

ferentiated feature matching method offers insights into the optimization and decision-making processes guiding the participation of FRs in regulating the regional power grid.

3) The optimal operation algorithm for multi-type FRs integrates adjusted boundaries and differentiated feature matching within the power grid. This algorithm demonstrates its ability to economically reduce imbalance power by 1.24% under practical operating conditions, effectively enhancing grid stability and economic efficiency.

In future research, avenues are opened for matching optimal FRs to multi-level power grids by the proposed method. Specifically, FRs with smaller feature differences could be prioritized for matching with urban-level and county-level power grids, which typically exhibit higher regulation demands. Conversely, FRs characterized by larger feature differences may be more suitable for matching with park-level and substation-level power grids, where regulation demands are comparatively lower. Moreover, this study will be further extended towards uncertainty modeling and analysis for the power grid.

REFERENCES

[1] D. Cao, W. Hu, J. Zhao *et al*., "Reinforcement learning and its applications in modern power and energy systems: a review," *Journal of Modern Power Systems and Clean Energy*, vol. 8, no. 6, pp. 1029-1042, Dec. 2020.

[2] N. Shang, Y. Ding, and W. Cui, "Review of market power assessment and mitigation in reshaping of power systems," *Journal of Modern Power Systems and Clean Energy*, vol. 10, no. 5, pp. 1067-1084, Sept. 2022.

[3] A. Nawaz, M. Zhou, J. Wu *et al*., "A comprehensive review on energy management, demand response, and coordination schemes utilization in multi-microgrids network," *Applied Energy*, vol. 323, p. 119596, Oct. 2022.

[4] B. Jiang and M. Y. Raza, "Research on China's renewable energy policies under the dual carbon goals: a political discourse analysis," *Energy Strategy Reviews*, vol. 48, p. 101118, Jul. 2023.

[5] Y. Fang, R. Fan, and Z. Liu, "A study on the energy storage scenarios design and the business model analysis for a zero-carbon big data industrial park from the perspective of source-grid-load-storage collaboration," *Energy Reports*, vol. 9, pp. 2054-2068, Sept. 2023.

[6] M. S. Javed, T. Ma, J. Jurasz *et al*., "Economic analysis and optimization of a renewable energy based power supply system with different energy storages for a remote island," *Renewable Energy*, vol. 164, pp. 1376-1394, Feb. 2021.

[7] R. Zhang, N. E. P. University, T. Jiang *et al*., "Day-ahead scheduling of multi-carrier energy systems with multi-type energy storages and wind power," *CSEE Journal of Power and Energy Systems*, vol. 4, no. 3, pp. 283-292, Sept. 2018.

[8] Y. Mi, Y. Chen, M. Yuan *et al*., "Multi-timescale optimal dispatching strategy for coordinated source-grid-load-storage interaction in active distribution networks based on second-order cone planning," *Energies*, vol. 16, no. 3, p. 1356, Jan. 2023.

[9] Z. Guo, H. Guo, Q. Hu *et al*., "Economic-based residential flexible resource allocation in microgrid," *Energy Reports*, vol. 7, pp. 99-109, Nov. 2021.

[10] S. Koohi-Fayegh and M. A. Rosen, "A review of energy storage types, applications and recent developments," *Journal of Energy Storage*, vol. 27, p. 101047, Feb. 2020.

[11] J. Li, D. Xu, J. Wang *et al*., "P2P multigrade energy trading for heterogeneous distributed energy resources and flexible demand," *IEEE Transactions on Smart Grid*, vol. 14, no. 2, pp. 1577-1589, Mar. 2023.

[12] Z. Li, Y. Xu, X. Feng *et al*., "Optimal stochastic deployment of heterogeneous energy storage in a residential multienergy microgrid with demand-side management," *IEEE Transactions on Industrial Informatics*, vol. 17, no. 2, pp. 991-1004, Feb. 2021.

[13] A. A. Pena, D. Romero-Quete, and C. A. Cortes, "Sizing and siting of battery energy storage systems: a Colombian case," *Journal of Modern Power Systems and Clean Energy*, vol. 10, no. 3, pp. 700-709, May 2022.

[14] X. Jiang, J. Chen, Q. Wu *et al*., "Two-step optimal allocation of stationary and mobile energy storage systems in resilient distribution networks," *Journal of Modern Power Systems and Clean Energy*, vol. 9, no. 4, pp. 788-799, Aug. 2021.

[15] X. Wang, K. Sun, X. Yang *et al*., "Optimal allocation method of hybrid energy storage capacity of multi-energy system under low-carbon background," *International Journal of Low-carbon Technologies*, vol. 18, pp. 820-828, Feb. 2023.

[16] Q. Yang, J. Li, R. Yang *et al*., "New hybrid scheme with local battery energy storages and electric vehicles for the power frequency service," *eTransportation*, vol. 11, p. 100151, Feb. 2022.

[17] H. Huang, Y. Li, and H. Liu, "Collaborative optimization strategy of source-grid-load-storage considering dynamic time series complementarity of multiple storages," *IET Generation*, *Transmission & Distribution*, vol. 17, no. 18, pp. 4007-4023, Sept. 2023.

[18] X. Jiang, Q. Li, Y. Yang *et al*., "Optimization of the operation plan taking into account the flexible resource scheduling of the integrated energy system," *Energy Reports*, vol. 8, pp. 1752-1762, Jul. 2022.

[19] H. Yang, Q. Yu, J. Liu *et al*., "Optimal wind-solar capacity allocation with coordination of dynamic regulation of hydropower and energy intensive controllable load," *IEEE Access*, vol. 8, pp. 110129-110139, Jan. 2020.

[20] X. Wu, K. Liang, and X. Han, "Renewable energy output tracking control algorithm based on the temperature control load state-queuing model," *Applied Sciences*, vol. 8, no. 7, p. 1099, Jul. 2018.

[21] E. G. Munoz, G. G. Alcaraz, and N. G. Cabrera, "Two-phase short-term scheduling approach with intermittent renewable energy resources and demand response," *IEEE Latin America Transactions*, vol. 13, no. 1, pp. 181-187, Jan. 2015.

[22] Y. Sun, X. Wang, Z. Li *et al*., "A source load value matching method based on matching degree in different spatial and temporal scales," in *Proceedings of 2020 7th International Conference on Information Science and Control Engineering*, Changsha, China, Dec. 2020, pp. 1623-1626.

[23] Y. Liu, Y. Qiao, S. Han *et al*., "Quantitative evaluation methods of cluster wind power output volatility and source-load timing matching in regional power grid," *Energies*, vol. 14, no. 16, p. 5214, Aug. 2021.

[24] W. Xu, R. Ma, C. Chen *et al*., "Day-ahead sharing model of multi-integrated energy service providers based on source-load matching degree," in *Proceedings of 5th International Workshop on Renewable Energy and Development*, Chengdu, China, Apr. 2021, pp. 1-5.

[25] M. H. Nozari, M. Yaghoubi, K. Jafarpur *et al*., "Development of dynamic energy storage hub concept: a comprehensive literature review of multi storage systems," *Journal of Energy Storage*, vol. 48, p. 103972, Apr. 2022.

[26] Z. Hu. (2020, Jan.). Energy storage for power system planning and operation. [Online]. Available: http://www.wiley.com/go/permissions

[27] M. Carrion and J. M. Arroyo, "A computationally efficient mixed-integer linear formulation for the thermal unit commitment problem," *IEEE Transactions on Power Systems*, vol. 21, no. 3, pp. 1371-1378, Aug. 2006.

[28] F. Nadeem, S. M. S. Hussain, P. K. Tiwari *et al*., "Comparative review of energy storage systems, their roles, and impacts on future power systems," *IEEE Access*, vol. 7, pp. 4555-4585, Dec. 2019.

Jie Li received the B.Eng. degree in electrical engineering and its automation from Sichuan University, Chengdu, China, in 2021. He is currently pursuing the M.Sc. degree in electrical engineering in Sichuan University. His research interests include energy storage allocation and operation.

Xiaoming Liu received the B.S. degree in electrical information engineering from Taiyuan University of Science and Technology, Taiyuan, China, in 2013. He is currently working as a Deputy Director in Economic and Technological Research Institute of State Grid Tibet Electric Power Company, Ltd., Lhasa, China. His research interests include new power system planning and operation.

Zixuan Zheng received the B.S. and Ph.D. degrees in electrical engineering from Sichuan University, Chengdu, China, in 2012 and 2017, respectively. He is currently working as an Associate Professor in the College of Electrical Engineering, Sichuan University. His research interests include power quality and operation and control of distributed energy resources.

Xianyong Xiao received the B.S., M.S., and Ph.D. degrees in electrical en-

gineering from Sichuan University, Chengdu, China, in 1990, 1998, and 2010, respectively. He is currently working as a Professor in the College of Electrical Engineering, Sichuan University. His research interests include power quality, smart distribution system, power system catastrophic event, uncertainty theory, and uncertain measures applied to power systems.

Shu Zhang received the B.S., M.S., and Ph.D. degrees in electrical engineering from Southwest Jiaotong University, Chengdu, China, in 2010, 2013, and 2018, respectively. Currently, she is currently working as a Research Assistant in the College of Electrical Engineering, Sichuan University, Chengdu, China. Her research interests include fault diagnosis and automation of distribution network, load analysis, and modelling by power disturbance data.

Hongzhi Gao received the A.S. degree in electrical engineering and its automation from Changsha University of Electric Power, Changsha, China, in 1999, and the M.S. degree in industrial and business management from Sichuan University, Chengdu, China, in 2006. His research interests include power dispatching management and new power system planning and operation.

Yongjun Zhou received the B.S. degree in hydraulic and hydropower engineering from Tibet University, Lhasa, China, in 2006, and the M.S. degree in electrical engineering from Wuhan University, Wuhan, China, in 2016. He is currently pursuing the Ph.D. degree in electrical engineering from Sichuan University, Chengdu, China. His research interests include modeling and stability analysis of load, power dispatching management and control.